Heliyon 5 (2019) e02927

Contents lists available at ScienceDirect

Heliyon

journal homepage: www.cell.com/heliyon

Research article

Assessment of heat transfer correlations in the sub-channels of proposed rod bundle geometry for supercritical water reactor

Seth Kofi Debrah [a,b], Edward Shitsi [a,b,*], Silas Chabi [a], Neda Sahebi [c]

[a] Department of Nuclear Engineering, Graduate School of Nuclear and Allied Sciences, University of Ghana, P.O. Box AE 1, Kwabenya, Accra, Ghana
[b] Ghana Atomic Energy Commission (GAEC), Nuclear Power Institute, P.O. Box LG 80, Legon-Accra, Ghana
[c] Institute of Nuclear Energy Safety Technology, CAS, FDS Team, P.O Box 1135, No. 350, Hefei, Anhui, 230031, China

ARTICLE INFO

Keywords:
Mathematics
Mechanical engineering
Nuclear engineering
Physics
Heat transfer correlations
Heat transfer enhancement
Heat transfer deterioration
Supercritical water-cooled reactor

ABSTRACT

There are heat transfer correlations for heat transfer analysis in single tube geometries after several experimental and theoretical heat transfer studies in these single tube geometries. This is not the case for heat transfer analysis in rod bundle geometry with regard to proposed square fuel assembly of the Supercritical-Water-Cooled Reactor (SCWR) European Atomic Energy (EURATOM) design. Thus limited heat transfer studies exist on rod bundle geometry at supercritical pressures. Heat transfer correlations with accurate prediction capabilities of coolant and wall temperatures will be helpful in carrying out heat transfer studies at supercritical pressures. This paper presents the performance of twelve selected heat transfer correlations assessed on the $1/8^{th}$ bare square fuel assembly of the SCWR EURATOM design using Simulation of Turbulent flow in Arbitrary Regions Computational Continuum Mechanics C ++ based code (STAR-CCM + CFD code). The obtained numerical results were compared with the results obtained by Waata numerical experimentation. Overall, the Cheng et al. correlation provided the most satisfying prediction for the wall temperatures in all the sub-channels and captured closely Wataa's Numerical data. The maximum wall temperature was obtained in sub-channel 9, the hottest sub-channel and exceeded the design limit 620 °C by 60 °C for the Cheng correlation. The difference in temperature between the hottest and coldest sub-channels 9 and 1 respectively was approximately 80 °C. It was found that Cheng correlation is best suited for heat transfer prediction in rod bundle geometry at supercritical pressures with regard to the proposed square fuel assembly of the SCWR EURATOM design. It was also found that the different numerical tools adopted for this study and Waata study were able to capture the trends of normal, enhanced and deteriorated heat transfer regimes normally observed at supercritical pressures. Nevertheless, experimental investigations involving rod bundles adopted in this study should be conducted to validate the results obtained numerically and address the inconsistency of the conclusions drawn when compared with Waata data and other similar studies.

1. Introduction

Thorough knowledge and understanding of heat transfer characteristics near and above the critical conditions of Pressure and Temperature are crucial to the successful design of Supercritical-Water-Cooled Reactor (SCWR). Heat transfer correlations with accurate prediction capabilities of coolant and wall temperatures in the three heat transfer regimes; normal heat transfer, enhanced heat transfer and deteriorated heat transfer regimes, is helpful in heat transfer prediction in various heat transfer systems. SCWR is the sixth candidate of the advanced, fourth generation nuclear reactor concepts proposed by the "Generation IV International Forum (GIF)" - a consortium of thirteen member countries that laid the groundwork for the fourth generation of nuclear energy systems (Policy Group, 2016). Operating with water at pressures higher than the thermodynamic critical pressure and temperature (22.064 MPa and 373.95 °C respectively). Thus, SCWRs are expected to have higher thermodynamic efficiency as compared to current Light Water Reactors (LWRs). Because of the unique properties and favorable heat and mass transfer characteristics, supercritical water has attracted great interest in many applications, such as fossil-fired power plants (Pioro et al., 2004; Farah et al., 2016; Schulenberg and Starflinger, 2012). At pressures above temperature-pressure critical point of water, two-phase flow of fluid is not observed at these supercritical pressures. The fluid flow is thus treated as single-phase flow. Issues such as critical heat flux and wall

* Corresponding author.
E-mail address: edwardshitsi@yahoo.com (E. Shitsi).

https://doi.org/10.1016/j.heliyon.2019.e02927
Received 27 June 2019; Received in revised form 9 November 2019; Accepted 22 November 2019

burnout observed at two-phase flow regime in the operation of Boiling Water Reactors BWRs are not observed in the operation of SCWRs. However, temperature limitations of fuel meat and cladding become fluid flow and heat transfer concerns at supercritical pressure conditions. Accurate wall temperature and heat transfer coefficient predictions in SCWR fuel assembly are therefore needed to guide the design and operation of SCWRs (Wang et al., 2017a,b).

Wang et al. (2017a,b) performed an experiment at supercritical pressures investigating boiling heat transfer to water in a 2 x 2 sub-channel of SCWR. Wall temperatures observed at sub-critical pressures were compared with that obtained at supercritical pressures. It was found out that subcritical wall temperatures could be less or more than the supercritical wall temperatures. This finding was influenced by the occurrence of departure from nucleate boiling and the value of heat flux to mass flux ratio. Gao and Bai (2017) performed numerical study investigating non-uniform heat transfer at supercritical pressures in a horizontal tube. The adopted governing equations were solved using finite volume method. Renormalization Group k-ε turbulence (RING k-ε) model was used to capture turbulence in the numerical simulation. The numerical results obtained compared well with the experimental data used for the validation, and based on this, the RING k-ε turbulence model was recommended for similar numerical studies. The results of the numerical study show that there exist a non-uniform heat transfer in a horizontal circular tube, and pressure and heat flux variations could influence heat transfer significantly in the tube at supercritical conditions. Shen et al. (2017) performed experimental and numerical study investigating heat transfer to water at supercritical pressure in a vertical tube. The dimensionless specific heat ratio, buoyancy and acceleration parameters were calculated. The variation of heat transfer coefficient with the dimensionless parameters was found to be significant. However, the Jackson buoyancy parameter does not show dependence on the heat transfer coefficient. Mockry et al. and Bishop et al. correlations performed well in predicting experimental heat transfer data among the six heat transfer correlations examined. It was found out that the mechanisms causing development of heat transfer enhancement and deterioration were due to combined effects of specific heat and buoyancy.

Gschnaidtner et al. (2018) carried out assessment of 11 heat transfer correlations at supercritical pressures. 12,000 experimental data points were used to evaluate these 11 heat transfer correlations. It was indicated that complex and implicit heat transfer correlations did not improve the prediction accuracy significantly, and it was recommended that simple and explicit heat transfer correlations like Cheng et al. correlation should be adopted in heat transfer prediction at supercritical pressures. It was also mentioned that more than 30 correlations were published in literature and different heat transfer correlation assessment methods such as recalculation and prediction methods produced contradictory results, and therefore more accurate heat transfer correlations should be developed. Zahlan et al. (2018) carried out heat transfer correlations assessment at supercritical pressures and indicated that experimental measurements for rod bundle geometries were scarce, and it was difficult carrying out experiments with water compared to carrying out experiments with CO_2, refrigerant-12 (R-12), and R-22. Li et al. (2018) carried out experimental heat transfer study at supercritical pressure investigating heat transfer in different geometries including tube, annular channel and rod bundle with grid spacers/wire wraps. The tube and annular geometries are referred to as simple geometries whereas the rod bundle geometries referred to as complex geometries. The findings obtained include:

1) There is enhanced heat transfer in larger tube geometry (tube geometry with larger cross-sectional flow area) with supercritical water, whereas the enhanced heat transfer is obtained in smaller rod bundle geometry (rod bundle geometry with smaller cross-sectional flow area);
2) Enhanced heat transfer occurs when the coolant water temperature is approaching pseudo-critical temperature in all the tube, annular and rod bundle geometries; and
3) Characteristics of heat transfer in different geometries are not same at supercritical pressures.

Qu et al. (2018) carried out both experimental and numerical studies in a smooth vertical tube at supercritical pressures investigating effects of specific heat ratio, buoyancy and acceleration parameters on heat transfer using ultra-supercritical water and found out SST k-ω turbulence model could predict heat transfer in enhanced and deteriorated heat transfer regimes, enhance heat transfer and deteriorated heat transfer are caused by effects of buoyancy and integral of specific in the boundary layer, non-uniform heat application could delay heat transfer deterioration occurrence in comparison with uniform heat application, and SST k-ω turbulence model could not accurately predict heat transfer in the deteriorated heat transfer regime and therefore need improvement. Hu and Gu (2018) performed an experimental study investigating heat transfer to water at supercritical pressures in annuli with spacers. It was found that blockage ratio, dimensionless distance, local enthalpy, heat flux, mass flux, pressure, and Reynolds number are the main parameters influencing heat transfer downstream from spacers at supercritical conditions. It was also found out that heat transfer predicting methods adopted at sub-critical pressures have limitations in predicting heat transfer at supercritical pressures.

Liu et al. (2019) carried out numerical study investigating heat transfer to water at supercritical pressures in vertical pipe using Direct Numerical Simulation (DNS) method. Effects of variation of thermo-physical properties, flow acceleration and buoyancy were studied. It was observed that flow acceleration caused by thermal expansion impairs turbulence but the presence of thermal boundary layer reduces the effects of flow acceleration on heat transfer at supercritical pressures. Heat transfer enhancement and deterioration are caused by buoyance effects as a results of growth and decay of turbulence. It was also observed that inaccurate prediction of heat transfer is caused by the failure of the adopted turbulence models to capture production of turbulence kinetic energy and turbulent Prandtl number. Du et al. (2019) carried out numerical study adopting SST turbulent model in a vertical tube at supercritical pressures. Effects of tube diameter on convective heat transfer were investigated. The findings obtained are 1) decreasing tube diameter improves heat transfer in the enhanced heat transfer region, 2) rising wall temperature in the deteriorated heat transfer region reduces by decreasing the tube diameter, and 3) there is close relationship between peak heat transfer coefficient and pseudo-critical temperature. It was indicated that significant variations in density and thermal acceleration caused by effect of inertia contribute to phenomenon of heat transfer deterioration at supercritical pressures. Kong et al. (2019) developed a new criterion for predicting heat transfer at the onset of heat transfer deterioration at supercritical pressures in vertical tubes with inner diameters varying from 3 to 38 mm. The new criterion valid for system pressures in the range of 22.5–31 MPa, mass fluxes in the range of 200–2150 kg/(m^2.s), and heat fluxes in the range of 148–1810 kW/m^2 with prediction accuracy of 94.25%. This prediction accuracy is higher than that of the existing criteria for predicting heat transfer at the onset of heat transfer deterioration. Pioro (2019) performed heat transfer study at supercritical pressures considering flow geometries (tubes, annulus, 3-and 7-rod bundles) and supercritical fluids (SCW, SC carbon dioxide and SC R-12). Pioro stated that the two (2) correlations Mokry et al., (2011) and Gupta et al. (2013) valid for only the normal and improved/enhanced heat transfer regimes. Pioro found out that the minimum onset of deteriorated heat flux that is observed in annulus, and 3- and

7-rod bundles is 1.6–1.8 times that of the bare tubes. Wang et al. (2019) performed an experimental study investigating heat transfer of water at supercritical pressure in a double pipe heat exchanger. It was found that total HTC increases with the mass flow rate, and the variation of the HTC of the outer tube with the increase of the mass flow rate is insignificant. The peak HTC decreases with the pressure increase. The temperature at which the peak HTC occurs is not the same as the PCT, and the difference between the two temperatures increases with pressure. And the difference between the two temperatures was attributed to the temperature variation at the heat transfer section and the variation of the physical properties (especially density) of the coolant. It was also found out that the effect of buoyancy at different pressures is significant in the PCT region. Chen et al. (2019) performed an experimental study investigating the spacer grid effects on transfer of heat to Freon R134a at supercritical pressure in a 19-rod bundle geometry. Enhanced heat transfer was maximum and reached its peak near the PCT region, and sub-critical heat transfer correlations were not able to capture this observation. Heat transfer enhancement effect by the spacer grid at supercritical conditions was similar to that at subcritical conditions. A new heat transfer correlation was developed to predict heat transfer in the PCT region. Lei et al. (2019) performed an experimental study investigating heat transfer to CO2 at supercritical conditions in a small tube. A new heat transfer correlation for heat transfer of supercritical CO2 using a deep learning method. It was found that different characteristics of heat transfer were observed for various heat fluxes at low mass flux. The enhanced heat transfer regime and the peak of heat transfer coefficient occurred in the low enthalpy region. The heat transfer coefficient decreases with pressure under low heat flux conditions, and heat transfer at low mass flux conditions is significantly influenced by buoyancy effect.

The supercritical fluid flow and heat transfer predictions using numerical tools is attracting a lot of attention recently because of the high pressure and temperature working conditions that limit the number of experimental studies carried out at these supercritical pressure conditions. Correlations on fluid flow and heat transfer are implemented in these numerical tools to obtain fluid flow and heat transfer data to complement similar limited experimental data (Shitsi et al., 2018). From the above literature review, there are few studies on 4-rod bundle geometry, and there is one study in literature on 7-rod bundle geometry by Dyadyakin and Popov (1977). Therefore, this paper seeks to present the performance of the twelve selected heat transfer correlations assessed on the 1/8th bare square fuel assembly (7-rod bundle geometry) of the SCWR EURATOM design using STAR-CCM + CFD code. The numerical results obtained were compared with the results obtained by Waata numerical experimentation.

2. Methodology

2.1. STAR-CCM + CAD and the system model descriptions

3D-CAD is a feature-based parametric modeler within STAR-CCM+ was used to generate the one-eighth geometry. Extruding and cutting operations were then executed on the created geometry. Parts and regions were subsequently assigned to the geometry for integration with meshing and simulation process. In this analysis, dimensions used for the model (in mm) were obtained from the square fuel assembly configuration design proposed by Hofmeister et al. (2005, 2007), as illustrated in Figure 1. Figure 1 shows the mesh scene of the computational geometry (Figure 1a) and a representation of Fuel rod and sub-channels in "1/8 assembly" (Figure 1b) created using STAR CCM + CAD. Optimum mesh size of 1, 177, 342 cells was obtained using meshing specifications including base size of 0.2 mm, prism layer thickness of 0.1 mm, near wall prism layer thickness of 0.1 mm and surface growth rate of 1.3 mm. Physics models and boundary specifications adopted are presented in

Table 1. Physics models and Boundary Specifications.

S/No	Physics Model	Specification
1	Space Model	3-Dimensional
2	Time Model	Steady State
3	Material	Water
4	Energy of State Model	Polynomial Density
5	Flow Model	Segregated Flow
6	Energy Model	Segregated Fluid
7	Viscous Regime Model	Turbulent
8	Turbulence Model	K-Omega
9	Wall Function	Low y^+ Treatment
10	Convection Scheme	2^{ND} Order Upwind
11	Inlet	Mass Flow
12	Outlet	Pressure
13	Wall Surface	Heat flux

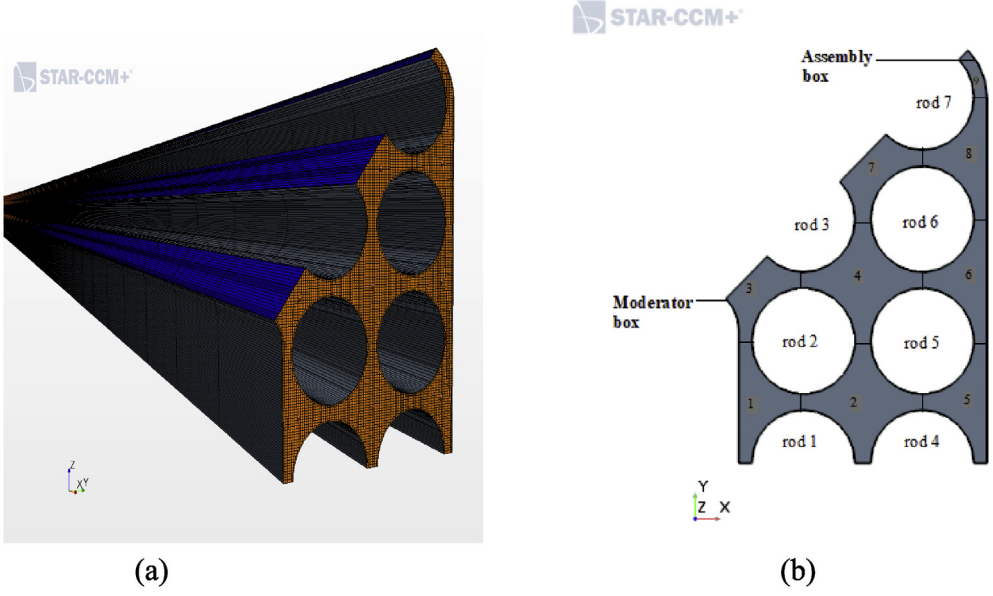

Figure 1. Mesh Scene of the Computational Geometry (a), and a representation of Fuel rod and sub-channels in "1/8 assembly" (b) created using STAR CCM + CAD.

Table 2. Dimensions used for creating a 1/8th FA geometry.

Square "2.1" Assembly type	Values
Number of moderator boxes per assembly (–)	1
Cladding outer diameter	8 mm
P/D	9.2
Number of fuel rods (–)	40
Active axial heated height	4.2 m
Fuel assembly box	
Length of the inner side	65.2 mm
Thickness of wall	1 mm
Length of the outer side	67.2 mm
Moderator box	
Length of the outer side	26.8 mm
Thickness of wall	0.3 mm
Length of the inner side	26.2 mm

Table 1. The Detailed dimensions of the 1/8th fuel assembly implemented in STAR-CCM + CAD are presented in Table 2.

2.2. Initial conditions

The numerical data used by Wataa (Waata, 2006) was implemented as input data for modelling 1/8th Fuel Assembly (FA) in the STAR-CCM + code. The fuel rod diameter of 8 mm, P/D ratio of 1.15 and 4.2 m as the active height of the heated section of the fuel assembly. The detailed dimensions of the FA is found in Waata (2006). A uniform heat flux of 650 kW/m^2 in the fuel rods was implemented in the STAR-CCM + code. The feed water temperature to the reactor pressure vessel was set at 280 °C and a total mass flow rate of 0.167 kg/s (601.2 kg/h). The operating pressure was 25 MPa with pseudo-critical temperature PCT of 384.9 °C. Inlet coolant temperature to the fuel assembly was set at 300 °C and in the sub-channels, the distribution was aimed at an average outlet temperature of 500–550 °C of this assembly. The water properties from National Institute of Standards and Technology (NIST) software Table was used to calculate physical properties of water applied for the SCW used in this analysis as a coolant (Lemmon et al., 2002).

2.3. Physical Models

The Physical Models adopted in this study includes Continuity equation, Momentum equations and Energy equation. The detailed treatments or descriptions of these Physical Models are given in the literatures, Podila and Rao (2014), CD-ADAPCO, 2015; Xi et al. (2014a, b), and Shitsi et al. (2017).

To reduce the computation time and effort for the simulation results of the FA to converge, symmetrical design advantage was utilized. Thus one-eighth (1/8th) the computational domain was considered and simulated. Four turbulence models were implemented and assessed with a view to choosing one turbulence model capable of capturing heat transfer characteristics of the coolant flow near, at and after the pseudo-critical region. Table 3 shows the selected turbulence models and their wall treatments. The treatments or description equations for turbulent kinetic energy κ, turbulent dissipation rate ε, and Specific dissipation rate ω, in the various turbulence models are detailed in the literatures, CD-ADAPCO, 2015; Xi et al. (2014b), and Shitsi et al. (2017).

Table 3. Turbulence models.

No.	Turbulence model	Type	Wall Treatment
1	Shear-Stress Transport (SST) Menter's	κ-ω	Low y+
2	Standard Wilcox	κ-ω	Low y+
3	Abe-Kondoh-Nagano (AKN) Low-Re	κ-ε	Low y+
4	Standard Lien's Low-Re	κ-ε	Low y+

2.4. Heat transfer correlation for supercritical conditions

Twelve different heat transfer correlations were considered and implemented in this study. This was to analyze their effects on the prediction of wall temperature in the proposed fuel assembly using STAR-CCM + code. The heat transfer correlations applied in this study are shown in Tables 4, 5, and 6.

In recent decades, many researchers have proposed heat transfer correlations at supercritical pressures. The most widely used heat transfer correlation for forced convection is the Dittus-Boelter correlation. Correlation of Bishop et al. which made use of Prandtl number was proposed to account for the effect of entrance region. In order to develop an accurate heat transfer correlation, experimental data covering a wide range of operating conditions was analyzed by Mokry et al., (2011). In order to improve heat transfer prediction at supercritical pressures compared with heat transfer prediction at subcritical pressures with constant fluid properties, acceleration parameter was proposed and implemented in Cheng et al. correlation.

As reported by Wang et al. (2017a,b), heat transfer correlations can be categorized into three types for supercritical fluids. The first category which performs well in the prediction of heat transfer in single phase fluids at subcritical conditions and is derived from the expression based on the Dittus and Boelter correlation (Dittus and Boelter, 1930). For the second category, a frictional factor has been added to the developed correlation equations for heat transfer in supercritical fluids that have been developed by Russian researchers. Most of the heat transfer correlations in the last category have been developed in recent years based on the "mechanisms of heat transfer at supercritical pressures". With a view to increasing an in-depth knowledge on the mechanisms of heat transfer enhancement and deterioration phenomena, some researchers have stated that buoyancy and thermal acceleration play dominant and significant roles in the prediction of wall temperatures (Cheng et al., 2009; Chen and Fang, 2014; Shitsi et al., 2017). The HTC in the supercritical water must be addressed prior to, and during the formulation and development of new empirical correlations. In addition, the integral effect of specific heat and buoyancy effect are the main reasons resulting in the abnormal heat transfer.

As can be seen in the Tables 4, 5, and 6, amid the 12 selected heat transfer correlations, only the Dyadyakin and Popov (1977) correlation was developed for rod bundle while the remaining 11 correlations were principally proposed and recommended for tubes.

3. Results and discussion

From the assessment results of the turbulence model results obtained, it can be inferred that the most suitable turbulence models capturing the coolant temperature obtained by Waata in this analysis were found to be SST κ-ω (Menter's) and standard (Wilcox) κ-ω as displayed in Figures 2, 3, 4, and 5. Nevertheless, SST κ-ω (Menter's) turbulence model was selected due to its widely used and recommendations are given by several researchers (Ampomah-Amoako and Ambrosini, 2013; Podila and Rao, 2014; Shitsi et al., 2017) who have carried out analysis on heat transfer behaviour at supercritical conditions related to SCWRs. Hence, the SST κ-ω (Menter's) turbulence model with a low y + wall treatment was used to carry out the numerical simulations in this study. It can be observed that the coolant and wall temperatures for the selected SST κ-ω (Menter's) turbulence model and that of Waata data flattened at the PCT region with temperature value of 384.9 °C. The coolant and wall temperature values begin to rise after the PCT region.

Figures 6, 7, 8, 9, 10, 11, 12, 13, 14, and 15 show average wall temperatures and heat transfer coefficients (HTCs) predicted and computed in sub-channels 1, 2, 4, 7 and 9 by the twelve (12) different heat transfer correlations namely Bishop et al. (1964), Mokry et al.

Table 4. Heat transfer correlations derived from the Dittus-Boelter equation.

References	Correlations	Flow Geometry	Applicability Range
Dittus and Boelter (1930)	$Nu_b = 0.023 Re_b^{0.8} Pr_b^{0.4}$	Tubes	Subcritical pressures
Griem (1996)	$Nu_b = 0.0169 Re_b^{0.8356} Pr_b^{0.432}$	Tubes	P = 0.4–27.4 MPa; G = 170–3000 kg/m^2 s; q = 420–8400 kW/m^2; t_b = 2.5–420 °C
Shitsman (1974)	$Nu_b = 0.023 Re_b^{0.8} Pr_{min}^{0.8}$	Tubes (D = 7.8, 8.2 mm)	P = 22.8–27.6 MPa; G = 651–3662 kg/m^2 s; q = 310–3460 kW/m^2; t_b = 282–527 °C
Bishop et al. (1964)	$Nu_b = 0.0069 Re_b^{0.9} \overline{Pr}_b^{0.66} \left(\frac{\rho_w}{\rho_b}\right)_x^{0.43} \left(1 + 2.4\frac{D_{hy}}{x}\right)$	Tubes (D = 2.5, 5.1 mm)	P = 22.6–29.4 MPa; G = 450–3000 kg/m^2 s; q = 280–1200 kW/m^2; H_{in} = 420–1400 kJ/kg
McAdams et al. (1950)	$Nu_b = 0.023 Re_f^{0.8} Pr_f^{0.33} \left(1 + 2.3\frac{D_{hy}}{l}\right)$	Tubes	P = 23–25 MPa, q = 0.3–0.6 MW/m^2, and G = 500–2500 kg/m^{2}s
Ornatsky et al. (1970)	$Nu_b = 0.023 Re_b^{0.8} Pr_{min}^{0.8} \left(\frac{\rho_b}{\rho_w}\right)^{0.3}$	Tube (D = 3 mm)	P = 0.8–24 MPa, t_b = 221 °C - 538 °C, q = 0.035–0.336 MW/m^2 and G = 75–224 kg/m^{2}s
Dyadyakin and Popov (1977)	$Nu_b = 0.021 Re_b^{0.8} \overline{Pr}_b^{0.7} \left(\frac{\rho_w}{\rho_b}\right)_x^{0.45} \left(\frac{\mu_b}{\mu_{in}}\right)^{0.2} \left(\frac{\rho_b}{\rho_{in}}\right)^{0.1} \left(1 + 2.5\frac{D_{hy}}{x}\right)$	Bundles (D_{hy} = 2.15–2.77 mm)	P = 24.5 MPa; G = 500–4000 kg/m^2 s; q < 4700 kW/m^2; t_b = 90–570 °C
Mokry et al. (2011)	$Nu_b = 0.0061 Re_b^{0.904} \overline{Pr}_b^{0.684} \left(\frac{\rho_b}{\rho_w}\right)^{0.564}$	Tube (D = 10 mm)	P = 24 MPa; G = 200–1500 kg/m^2 s; q = 70–1250 kW/m^2; tin = 320–350 °C
Gupta et al. (2013)	$Nu_b = 0.0061 Re_w^{0.94} \overline{Pr}_w^{0.76} \left(\frac{\mu_w}{\mu_b}\right)^{0.4} \left(\frac{\rho_b}{\rho_w}\right)^{0.16}$	Tube (D = 10 mm)	P = 24 MPa; G = 200–1500 kg/m^2 s; q = 70–1250 kW/m^2; tin = 320–350 °C

Table 5. Heat transfer correlations with frictional factor incorporated.

References	Correlation	Flow Geometry	Applicability Range
Petukhov et al. (1983)	$St = \frac{Nu}{Re \cdot Pr} = \frac{(\xi/8)}{12.7\sqrt{(\xi/8)}(\overline{Pr}_b^{2/3} - 1) + 1 + \frac{900}{Re}}$, where $\xi = \frac{1}{(1.82 log Re_b - 1.64)^2} \left(\frac{\rho_w}{\rho_b}\right)^{0.4} \left(\frac{\mu_w}{\mu_b}\right)^{0.2}$	Tubes, upwards, downwards and horizontal (D = 8 mm, L = 1.67 m)	P = 7.7–8.9 MPa; G = 1000–4100 kg/m^2 s; q = 384–1053 kW/m^2; t_b = 0–80 °C
Krasnoshchekovet al. (1967)	$Nu_b = Nu_o \left(\frac{\mu_b}{\mu_w}\right)^{0.11} \left(\frac{\lambda_b}{\lambda_w}\right)^{0.3} \left(\frac{\overline{C}_p}{C_{p_b}}\right)^{0.35}$ $Nu_o = \frac{(\xi/8) Re_b \overline{Pr}}{12.7\sqrt{(\xi/8)}(\overline{Pr}_b^{2/3} - 1) + 1.07}$, where $\xi = (1.82 log Re_b - 1.64)^2$	Tubes (D = 1.6–20 mm)	$2\times10^4 < Re_b < 8.6\times10^5$, $0.85 < \overline{Pr}_b < 65$: $0.90 < \mu_b/\mu_w < 3.60$; $1.00 < k_b/k_w < 6.00$ and $0.07 < \overline{C}_p/C_{p_b} < 4.50$

Table 6. Heat transfer correlations taking into account buoyancy and thermal acceleration.

References	Correlation	Flow Geometry	Applicability Range
Cheng et al. (2009)	$Nu_b = 0.023 Re_b^{0.8} Pr_b^{0.33} F$, where $F = \min(F_1, F_2)$, $F_1 = 0.85 + 0.766(\pi_A \cdot 10^3)^{2.4}$ $F_2 = \frac{0.48}{(\pi_{A_{pc}} \cdot 10^3)^{1.55}} + 1.21\left(1 - \frac{\pi_A}{\pi_{A_{pc}}}\right)$ and $\pi_A = \frac{\beta_b q}{G C_p}$	Tubes (D = 10, 20 mm)	P = 22.5–25 MPa; G = 700–3500 kg/m^2 s; q = 300–2000 kW/m^2; t_b = 300–450 °C
Chen and Fang (2014)	$Nu_b = 0.46 Re_b^{0.16} \left(\frac{Pr_w}{Pr_b}\right)^{0.1} \left(\frac{\nu_w}{\nu_b}\right)^{-0.55} \left(\frac{\overline{C}_p}{C_{p_b}}\right)^{0.88} \left(\frac{Gr_b^*}{G_r}\right)^{0.81}$	Tubes (D = 6–26 mm)	P = 22–34.3 MPa; G = 201–2500 kg/m^2 s; q = 129–1735 kW/m^2; H_b = 278–3169 kJ/kg

(2011), Cheng et al. (2009), Dyadyakin and Popov (1977), Ornatsky et al. (1970), Shitsman (1974), Dittus Boelter (1930), McAdams et al. (1950), Griem (1996), Kranoshchekov et al. (1967), Gupta et al. (2013) and Petukhov et al. (1983). These wall temperatures and HTCs are compare with Wataa's numerical data of wall temperatures and HTCs. Results and findings on the sub-channels 3, 5, 6 and 8 are similar to those of the sub-channels 1, 2, 4, 7 and 9, and therefore, not presented in the following discussions.

The average wall temperatures and heat transfer coefficients obtained by Waata were computed using the Bishop Heat transfer correlation based on the Dittus Boelter correlation. Waata made use of sub-channel code STAFAS and Monte Carlo Code MCNP for thermal hydraulic and neutronic studies which involved iterative procedure. Cheng et al. (2003) developed the STAFAS code. In order to restrict the thermal hydraulic and neutronic analyses to the 1/8 of a single assembly which was shown in Figure 1, assumptions such as perfect neutron reflection and symmetric power and density distributions were made in the fuel assembly (Hofmeister et al., 2007). The original STAFAS code included only the Dittus Borlter correlation. Bishop correlation was implemented for supercritical water heat transfer in smooth tubes. Cheng and Schulenberg (2001) carried out literature review and made recommendation that Bishop correlation could be applied for HPLWR analysis. Waata (2006) contains detailed information on the coupled sub-channel analysis.

Figures 6 and 7 show comparisons of the wall temperatures and HTCs computed using the twelve selected correlations with that of Waata's data respectively. In Figure 6, it was observed that in the NHT region all the twelve correlations did not closely capture the wall temperatures obtained by Waata. However, in the enhanced heat transfer region, most of the correlations closely captured the wall temperatures obtained by Waata except the Cheng et al., McAdams and Petukhov correlations which slightly overestimated the Waata's wall temperatures. In the deteriorated heat transfer region, the Cheng et al. correlation followed by the McAdams, and Dyadyakin and Popov correlations captured closely the Wataa's wall temperature, from 1.7 m to about 3.8 m, except towards the outlet of the sub-channel where wall temperatures obtained by 12 correlations were more than that of Waata's. On the other hand, the Gupta correlation underestimated the wall temperature obtained by

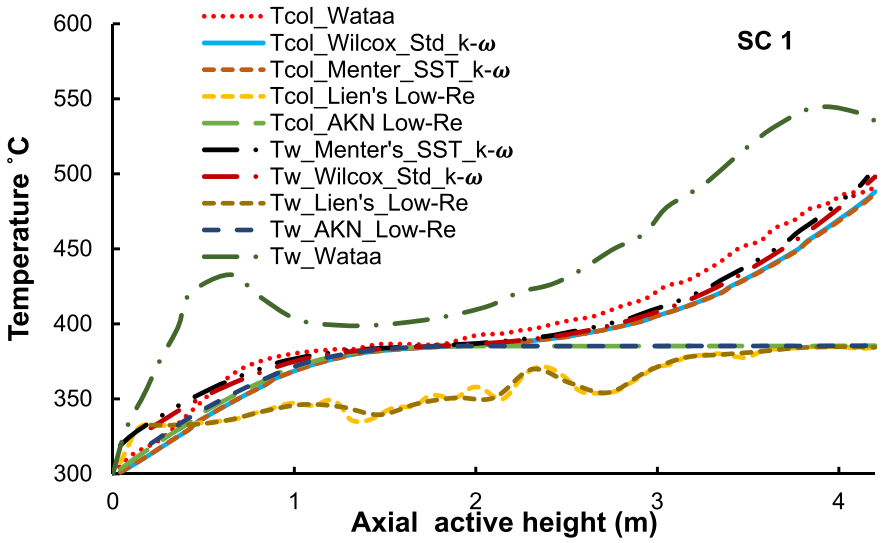

Figure 2. Temperature profiles in SC 1 of a square fuel assembly.

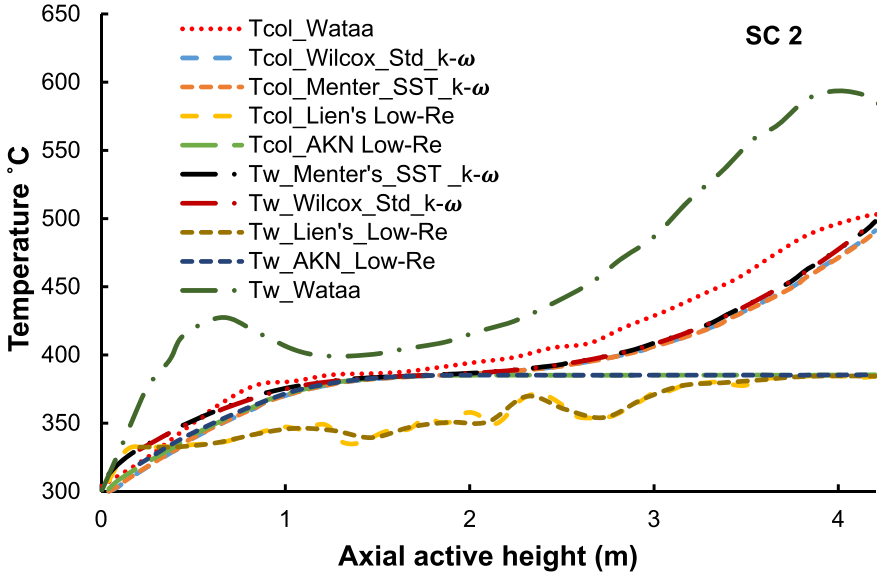

Figure 3. Temperature profiles in SC 2 of a square fuel assembly.

Waata, this was followed by the Shitsman and Ornatsky correlations in the HTD region.

In the case of HTCs observed in Figure 7, most of the correlations closely captured the HTC computed by Waata at the entrance part of the sub-channel. However, there was a shift in the location of the maximum peaks (between 1.68 m and 2 m) for the twelve-correlation compared to the HTC computed by Waata (1.3 m) along the active length of the sub-channel. Beyond 2.0 m, the Cheng et al. correlation closely captured the Waata HTC, `followed by the McAdams, Dittus Boelter, Griem, and Dyadyakin and Popov correlations. The Gupta correlation over-estimated the HTC as observed in Figure 7. The NHT region is observed at the inlet section where all the correlations closely predicted the Waata HTC data (from 0.0 m to 0.8 m of the active length of the sub-channel). This NHT region is followed by HTE where the HTC values start to increase up to the point where the peak of each heat transfer correlation is located. The region after the HTE region is the HTD region.

The following set of graphical results presents the rest of comparisons of the wall temperature profiles computed by the 12 selected correlations with the wall temperatures obtained by Waata in sub-channels 2, 4, 7 and 9.

Accordingly, it was observed that in all the 5 sub-channels analyzed, the wall temperatures computed by the Cheng et al. correlation consistently and closely captured Waata's obtained wall temperatures in the HTD region from 2.0 m to about 3.8 m along the active length. In sub-channel 2, the Cheng et al. correlation was followed by the Dyadyakin and Popov, McAdam's, and Petukhov correlations (Figure 8). A similar trend of the estimation of the wall temperatures obtained by the correlations and compared with the Waata data was shown in Figure 9 (results of sub-channel 4), however towards the outlet of the sub-channel only the wall temperatures computed by the Cheng et al., and Dyadyakin and Popov correlations were more than that of Waata's in both sub-channels 2 and 4 (Figures 8 and 9). In addition, it was also observed that the Cheng et al. correlation overestimated the wall temperature obtained by Waata in the HTE region, in sub-channels 2 and 4. The Gupta, Shitsman, Mokry, Krasnoshchekov and Protopopov correlations under-estimated the wall temperature obtained by Waata in the HTD region in sub-channel 2 (Figure 8). A similar trend was observed in sub-channel 4, except for the

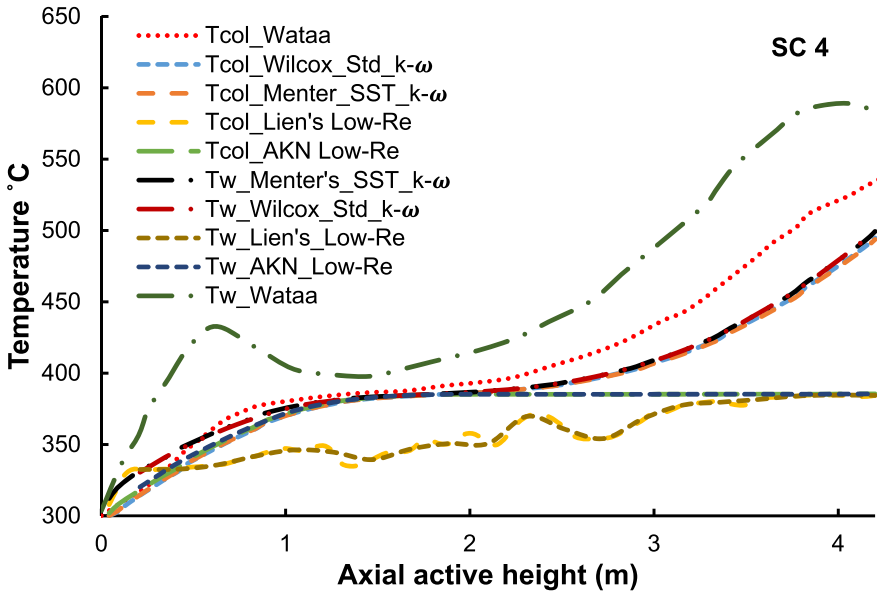

Figure 4. Temperature profiles in SC 4 of a square fuel assembly.

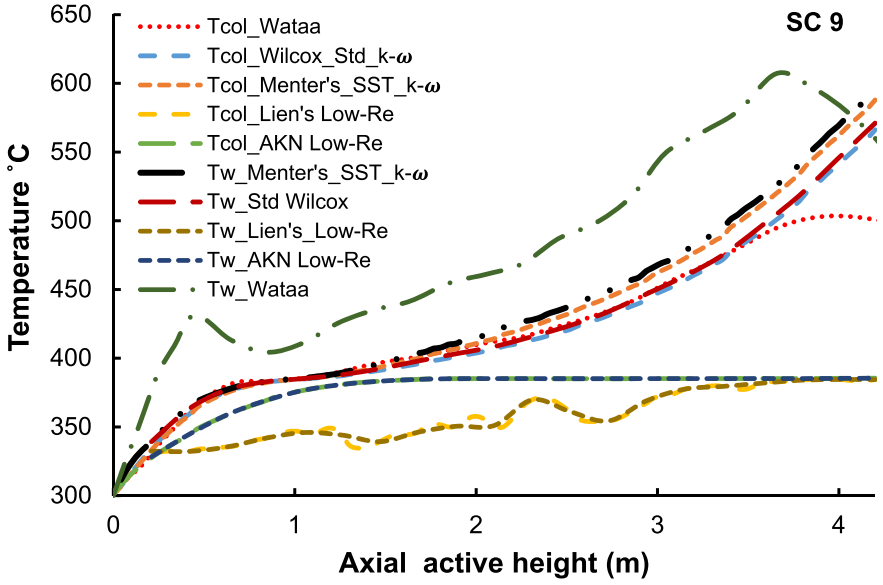

Figure 5. Temperature profiles in SC 9 of a square fuel assembly.

Gupta correlation which closely estimated the wall temperatures obtained by Waata (Figure 9).

In sub-channels 7, as observed in the other sub-channels, the Petukhov and Cheng et al. correlations slightly overestimated the wall temperature obtained by Waata in the HTE region. In the HTD region, the result of Cheng et al. correlation agreed with the Wataa's data, from 1.68 m to 3.78 m in sub-channel 7 (see Figure 10). However, in sub-channel 9, both the results of Cheng et al. and Kranoshchekov and Protopopov were very close to the results of the Waata in the HTD region (see Figure 11). Moreover, in the upper part of the sub-channel 9, all the wall temperatures computed by the 12 selected correlations in the sub-channel were more than the wall temperature obtained by Waata. Nevertheless, in sub-channel 7 only the Petukhov, Cheng et al. and Dyadyakin and Popov wall temperatures were more than the Waata's wall temperature in the upper part of the channel.

Furthermore, for all the five (5) sub-channels in the NHT region, it was observed that the twelve correlations did not favorably estimate the wall temperature obtained by Waata. In the HTE region of sub-channel 9, almost all the correlations captured the wall temperature trend obtained by Waata, except the Gupta correlation which slightly under-estimated it. It was observed also that almost all the 12 twelve correlations closely predicted the Waata numerical wall temperature at the PCT region of 384.9 °C. The trends of the wall temperatures observed at the PCT region flattened around 384.9 °C indicating maximum enhanced heat transfer in this PCT region. This observation was also made in other experimental and numerical studies including Xi et al. (2014a); Gu et al. (2015a, b); Wang et al. (2014); Gu et al. (2016); Shitsi et al. (2017); Li et al. (2018); and Kong et al. (2019). It is interesting observing that both the coolant and wall temperatures tend to flatten at the PCT region around the PCT value with the coolant temperatures below the wall temperatures as shown in the figures. The maximum deviations of the wall temperatures estimated by the 12 twelve correlations from the Waata wall temperature were observed at the HTD region towards the upper part of the sub-channels (or the outlet of the sub-channels). Thus most of the 12 heat transfer

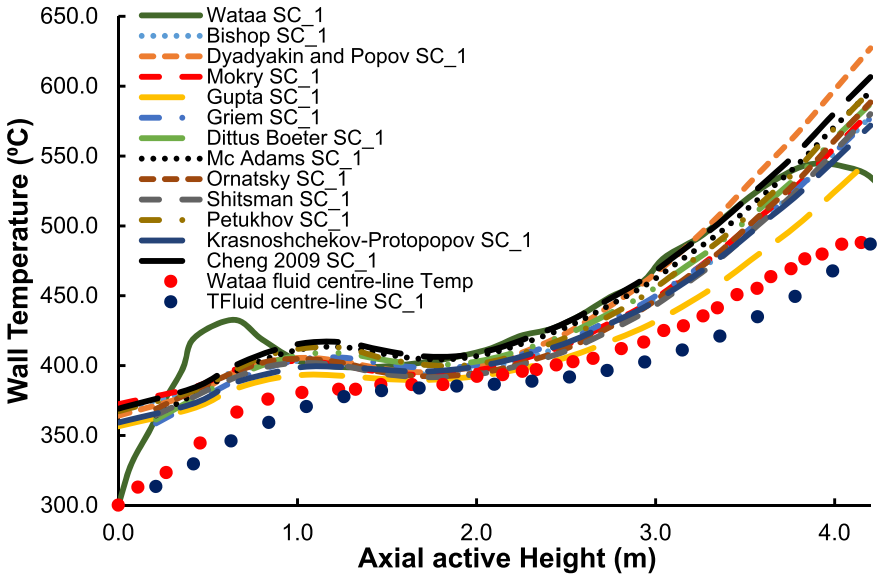

Figure 6. Simulation results for selected heat transfer correlations showing the wall temperature profiles in SC 1.

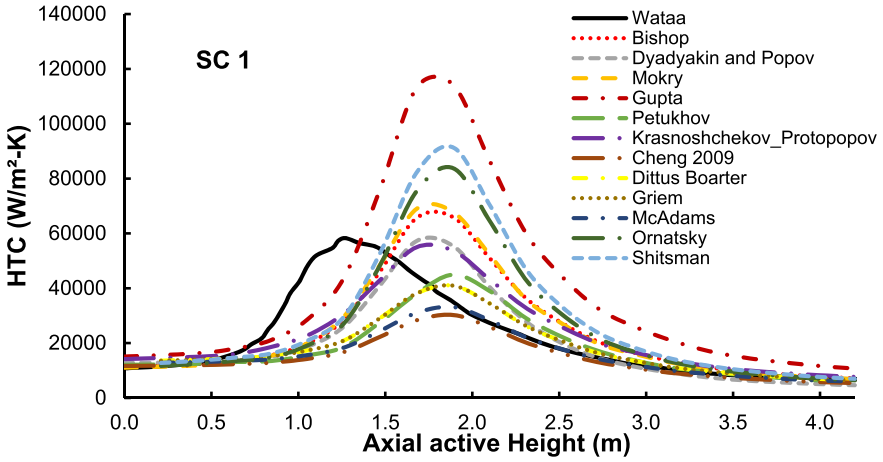

Figure 7. Simulation results for selected heat transfer correlations showing the HTC profiles in SC (1).

correlations predicted the Waata data quite well in the enhanced heat transfer region compared to the prediction in the deteriorated heat transfer region.

In general, based on Cheng et al. correlation, it was observed that the maximum wall temperature computed slightly exceeds the design allowable limit of 620 °C by an average of 10 °C in SC (1) (the coldest SC), SC (2) and SC (4), as captured in Figures 6, 8, and 9 respectively. In sub-channels 7, the allowable limit temperature was exceeded by 35 °C (Figure 10), while in sub-channel 9 (the hottest SC) the deviation from the design limit was a little more than 80 °C as observed in Figure 11. The difference in temperature between the hottest and coldest sub-channels 9 and 1 respectively was approximately 80 °C. The maximum wall temperature was obtained in sub-channel 9, the hottest sub-channel and exceeded the design limit 620 °C by 60 °C for the Cheng correlation while for the other correlations it was more. It was also observed that the different numerical tools adopted in the current study and in the study of Waata are able to predict the Normal, Enhanced and Deteriorated heat transfer regimes normally observed in the heat transfer systems at supercritical pressures.

The results for the HTCs in sub-channel 2, 4, 7, and 9 are presented in Figures 12, 13, 14, and 15.

In sub-channel 2 (see Figure 12), most of the correlations estimated closely the HTC data obtained by Waata at the inlet part of the sub-channel except the Krasnoshchkov and Protopopov, and Cheng et al. correlations' results. In the half part of the subchannel towards the outlet, the Cheng et al., McAdams, and Dyadyakin and Popov correlations closely estimated the HTC obtained by Waata. It was observed that there was a shift in the location of the maximum peak (between 1.7 m and 2.0 m) for HTCs computed by the twelve different correlations, compared to that of Waata's (1.2 m). The Cheng et al. correlation had the lowest peak while the Shitsman, Bishop and Gupta correlations had the highest peak in sub-channel 2. The peak of the Dyadyakin and Popov, as well as that of Krasnoshchkov and Protopopov correlations, was close the HTC's peak obtained by Waata.

Figure 13 also shows a similar trend of HTC profile observed in sub-channel 4, except that the Cheng et al. and McAdams correlations showed a good agreement with Waata's computed HTCs at the entrance of the sub-channel and from 2.0 m to 4.2 m. Similarly, only the Gupta correlation had the highest peak while the Bishop, and Kranoshchekov and Protopopov correlations have the similar peak with the Waata's computed HTC result.

Figure 14 shows HTC profiles observed in sub-channel 7. The twelve correlations predicted HTC values close to that of the Waata in the NHT

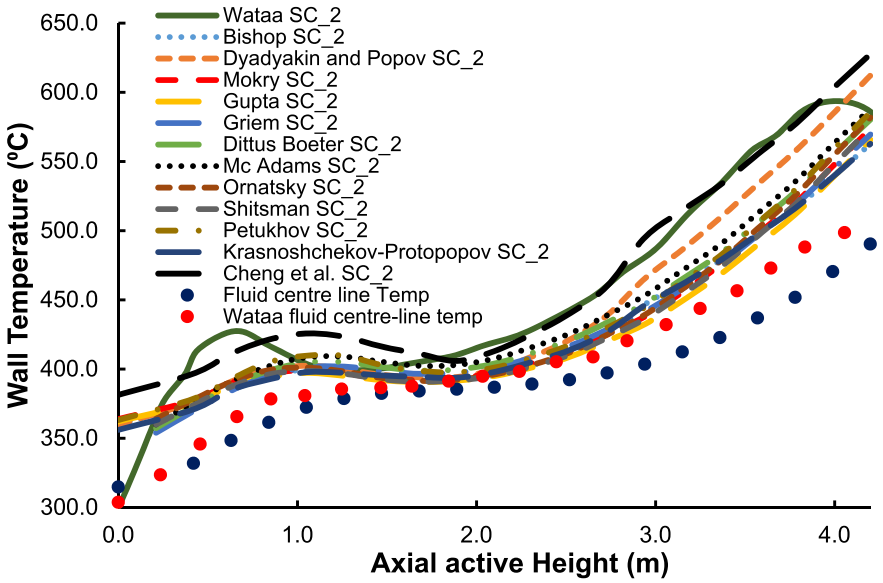

Figure 8. Simulation results for selected heat transfer correlations showing the wall temperature profiles in SC 2.

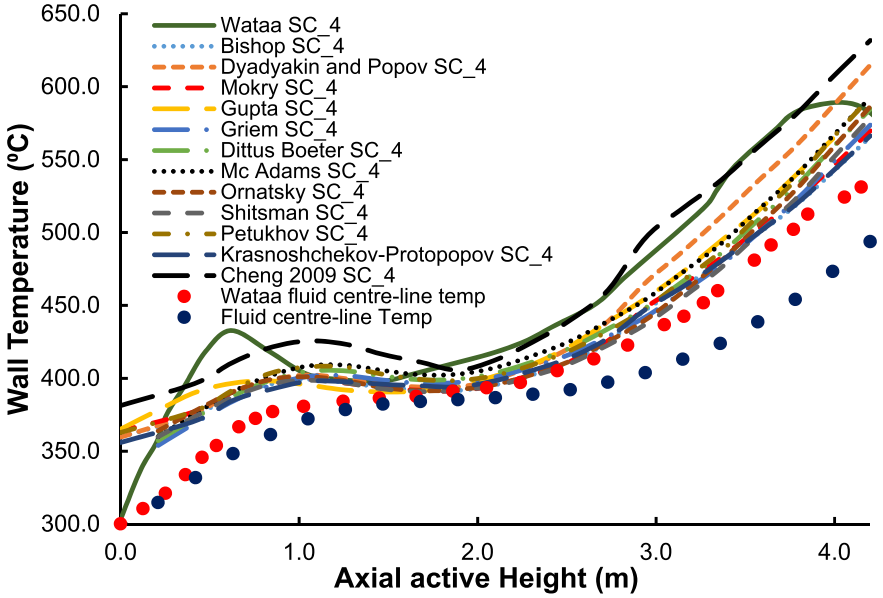

Figure 9. Simulation results for selected heat transfer correlations showing the wall temperature profiles in SC 4.

region observed at the inlet section of the sub-channel. Maximum deviations in the HTC values observed in the HTE region where the HTC peak for each heat transfer correlation was located. The HTC peaks of Gupta et al., Mokry et al., Bishop et al., Shitsman, Ornatsky, and Dyadyakin and Popov correlations were above that HTC peak of the Waata data. The remaining heat transfer corrlations have their HTC peaks below that of the Waata data. Heat transfer from the fuel rods to the coolant is at its maximum in this HTE region. This HTE region is followed by HTD region where heat transfer from the fuel rods to the coolant started to reduce to its minimum towards the end of the sub-channels for all the twelve heat transfer correlations.

A similar trend of HTC results was also observed in sub-channel 9 (see Figure 15) computed using the twelve different correlations and compared with the HTC result obtained by Waata. The peaks obtained by Bishop, Dyadyakin and Popov, and Mokry correlations were close to the peak of the Waata data. However, it was observed that the Gupta correlation significantly overestimated the HTC result obtained by Waata. Gupta correlation had the highest peak followed by Shitsman, Ornatsky and McAdams correlations, while the peaks of Kranoshchekov and Protopopov, Petukhov, Griem, Cheng et al. and Dittus Boelter correlations were below the peak obtained by Waata but at different locations.

It was also observed that there was a shift in the location of the peak for HTCs computed by the twelve different correlations, compared to the Waata's HTCs. In all the five sub-channels, the Gupta correlation had the highest peak, this was followed by the Shitsman correlation except in SC (4) (see Figure 9). The maximum value of the HTC was approximately 146 kW/m^2 in sub-channel 9 and the minimum HTC value was approximately 102 kW/m^2 in sub-channel 2, obtained by the Gupta correlation. For Cheng et al. correlation, the value of the HTC was approximately 41 kW/m^2 in sub-channel 9 and approximately 32 kW/m^2 in sub-channel 2. It was also observed that the peak location varied between 1.0 m and 2.0 m for the12 selected heat transfer correlations in all the individual sub-channels. Studies such as Gu et al. (2015a, b); Wang et al. (2014); Gu et al. (2016), Gao and Bai (2017); Shen et al. (2017); Li et al. (2018);

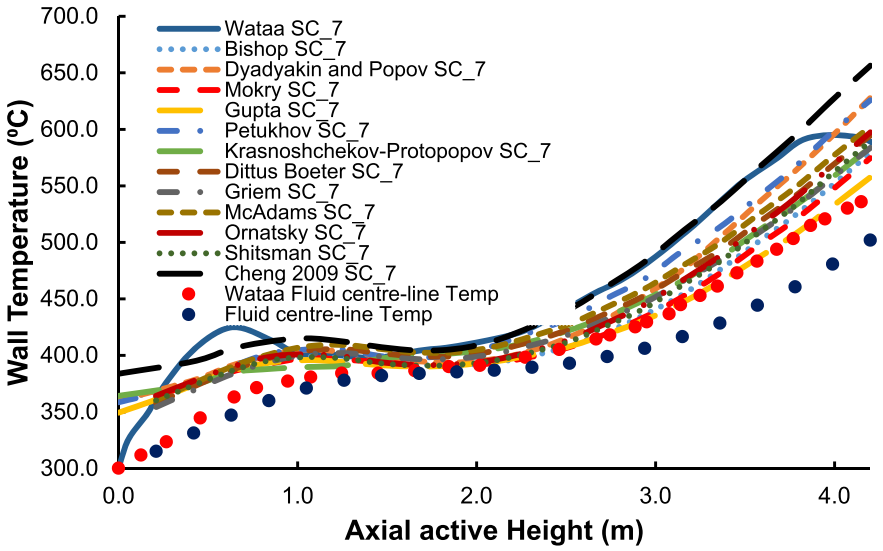

Figure 10. Simulation results for selected heat transfer correlations showing the wall temperature profiles in SC 7.

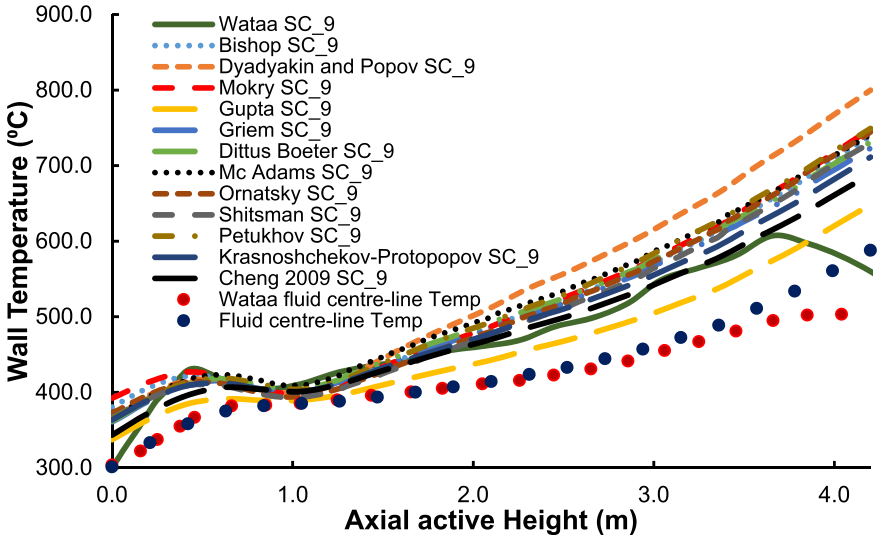

Figure 11. Simulation results for selected heat transfer correlations showing the wall temperature profiles in SC 9.

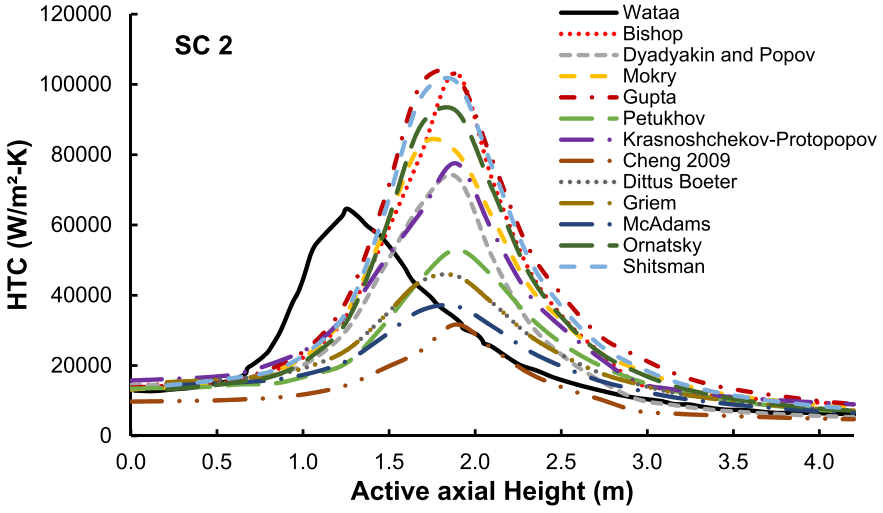

Figure 12. Simulation results for selected heat transfer correlations showing the HTC profiles in SC (2).

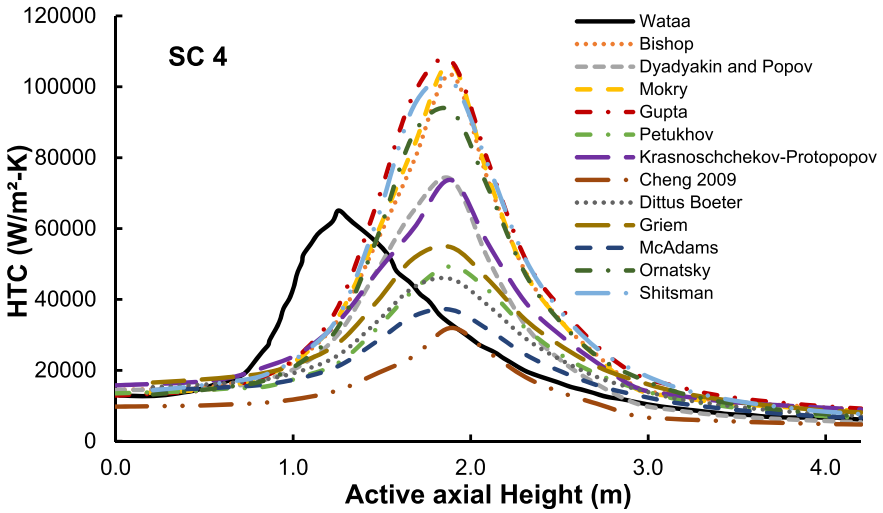

Figure 13. Simulation results for selected heat transfer correlations showing the HTC profiles in SC (4).

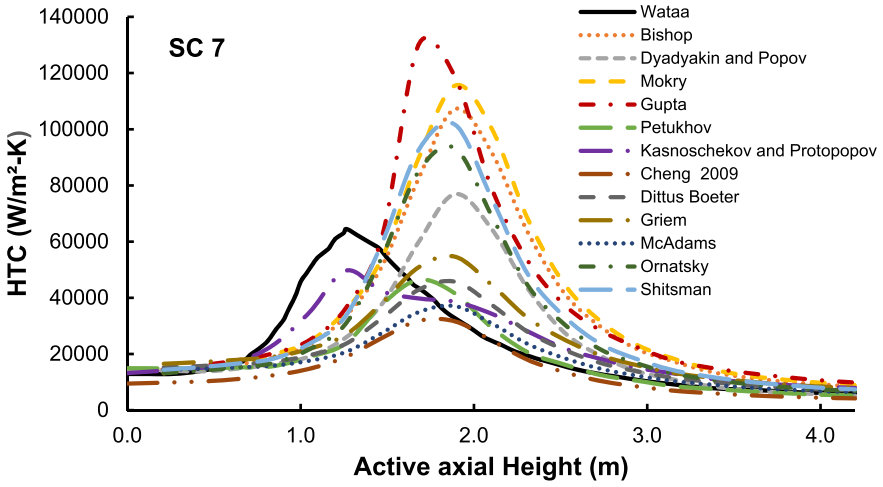

Figure 14. Simulation results for selected heat transfer correlations showing the HTC profiles in SC (7).

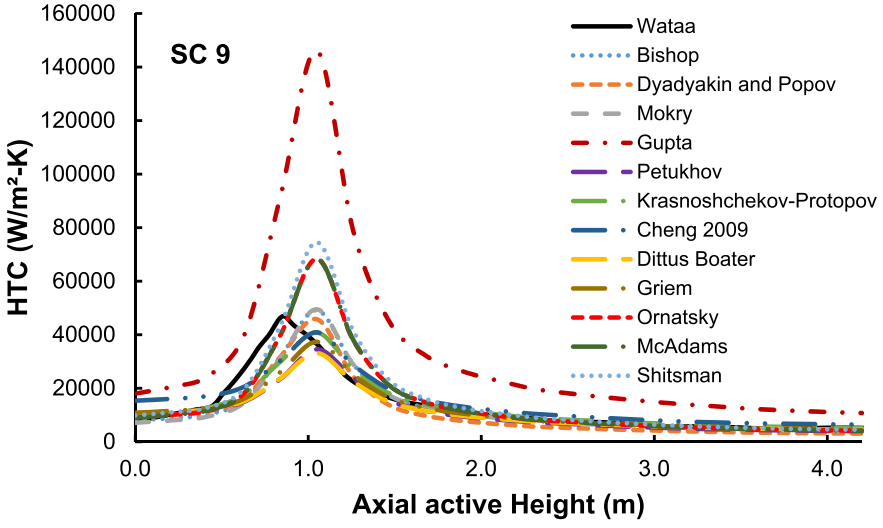

Figure 15. Simulation results for selected heat transfer correlations showing the HTC profiles in SC (9).

Kong et al. (2019); Du et al. (2019); and Lei et al. (2019) obtained similar shape of the HTC profile obtained in this study.

It can be observed that both the coolant and wall temperature results of this study, and that of the Waata study flattened at the PCT region with a temperature value of 384.9 °C (PCT value at 25 MPa). Thus the coolant and wall temperature values of the two numerical studies are close or equal to 384.9 °C in all the coolant and wall temperature results presented in Figures 2, 3, 4, 5, 6, 8, 9, 10, and 11, an indication that the results obtained in these two numerical studies might not deviate significantly from the experimental results yet to be obtained. For most of good experimental and numerical studies on heat transfer to water at supercritical pressures, the trend of the wall temperatures obtained flattened at this PCT region with the values of the coolant and wall temperatures close or equal to the PCT value. Heat transfer coefficient prediction of SCW is challenging due to the steep and non-linear variations in its thermo-physical properties. Near the pseudo-critical point, the density, thermal conductivity, and viscosity fall drastically whereas the specific heat experiences a sharp peak. It can be observed that none of the correlations tested in this analysis is most reliable heat transfer correlation providing favorable prediction in all the sub-channels, hence there is still no consistent conclusion on the best performing heat transfer correlation. This leaves room for improvement and modification on the best performing correlations in this analysis.

4. Conclusions

This study seeks to present the performance of twelve selected heat transfer correlations assessed on the 1/8th bare square fuel assembly of the SCWR EURATOM design. The STAR-CCM + CFD Code was used for this study. SST κ-ω turbulence model was selected among other turbulence models implemented in the code. The obtained results from this work were compared with the results obtained by Waata numerically. Overall, the Cheng et al. correlation provided the most satisfying prediction for the wall temperatures in all the sub-channels and captured closely Waata's Numerical data. This was followed by the McAdams correlation, but the Dyadyakin and Popov, and the Petukhov correlations also yielded results close to Waata data. The maximum wall temperature was obtained in sub-channel 9, the hottest sub-channel and exceeded the design limit 620 °C by 60 °C for the Cheng correlation while for the other correlations it was more. The difference in temperature between the hottest and coldest sub-channels 9 and 1 respectively was approximately 80 °C. It was also found that the different numerical tools adopted for this study and Waata study were able to capture the trends of normal, enhanced and deteriorated heat transfer regimes normally observed at supercritical pressures.

Declarations

Author contribution statement

Seth Kofi Debrah: Conceived and designed the experiments; Performed the experiments; Analyzed and interpreted the data; Contributed reagents, materials, analysis tools or data; Wrote the paper.

Edward Shitsi, Silas Chabi & Neda Sahebi: Performed the experiments; Analyzed and interpreted the data; Contributed reagents, materials, analysis tools or data.

Funding statement

This research did not receive any specific grant from funding agencies in the public, commercial, or not-for-profit sectors.

Competing interest statement

The authors declare no conflict of interest.

Additional information

No additional information is available for this paper.

Acknowledgements

Cd-Adapco is acknowledged for providing a free license and technical support in making this study possible. Prof. Walter Ambrosini of University of Pisa is hereby acknowledged for his cubic spline program development for attaining the properties of water and other coolants.

References

Ampomah-Amoako, E., Ambrosini, W., 2013. Developing a CFD methodology for the analysis of flow stability in heated channels with fluids at supercritical pressures. Ann. Nucl. Energy 54, 251–262.

Bishop, A.A., Sandberg, R.O., Tong, L.S., 1964. Forced convection heat transfer to water at near critical temperatures and supercritical pressures. WCAP 2056. Part-III-B.

CD-ADAPCO, 2015. User Guide STAR-CCM+,Version 10.06.009. New York.

Chen, W.W., Fang, X.D., 2014. A new heat transfer correlation for supercritical water flowing in vertical tubes. Int. J. Heat Mass Transf. 78, 156–160.

Chen, J., Xiong, Z., Xiao, Y., Gu, H., 2019. Experimental study on the grid-enhanced heat transfer at supercritical pressures in rod bundle. Appl. Therm. Eng.

Cheng, X., Schulenberg, T., 2001. Heat transfer at supercritical pressures-literature review and application to an HPLWR. Wissenschaftliche Berichte (Tech. Report), FZKA 6609. Forschungszentrum Karlsruhe, Mai.

Cheng, X., Schulenberg, T., Bittermann, D., Rau, P., 2003. Design analysis of core assemblies for supercritical pressure conditions. Nucl. Eng. Des. 223, 279–294.

Cheng, X., Yang, Y.H., Huang, S.F., 2009. A simplified method for heat transfer prediction of supercritical fluids in circular tubes. Ann. Nucl. Energy 36, 1120–1128.

Dittus, F.W., Boelter, L.M.K., 1930. Heat Transfer in Automobile Radiators of Tubular Type, 13. University of California, Publications of Engineering, pp. 443–461.

Du, X., Lv, Z., Zhao, S., Qiu, Q., Zhu, X., 2019. Numerical analysis of diameter effects on convective supercritical water flow in a vertical round tube. Appl. Therm. Eng. 160, 114095.

Dyadyakin, B.V., Popov, A.S., 1977. Heat transfer and thermal resistance of tight seven-rod bundle cooled with water flow at supercritical pressures. Trans. VTI 11, 244–253.

Farah, A., Harvel, G., Pioro, I., 2016. Analysis of computational fluid dynamics code FLUENT capabilities for supercritical water heat-transfer applications in vertical bare tubes. J. Nucl. Eng. Radiat. Sci. 2 (3), 031016.

Gao, Z., Bai, J., 2017. Numerical analysis on nonuniform heat transfer of supercritical pressure water in horizontal circular tube. Appl. Therm. Eng.

Griem, H., 1996. A new procedure for the prediction of forced convection heat transfer at near- and supercritical pressure. Heat Mass Transf. 31, 301–305.

Gschnaidtner, T., Schatte, G.A., Kohlhepp, A., Wang, Y., Wieland, C., Spliethoff, H., 2018. "A new assessment method for the evaluation of supercritical heat transfer correlations, particularly with regard to the "multiple/no solutions" problem". Therm. Sci. Eng. Prog. 7, 267–278.

Gu, H.Y., Li, H.B., Hu, Z.X., Liu, D., Zhao, M., 2015a. Heat transfer to supercritical water in a 2 × 2 rod bundle. Ann. Nucl. Energy 83, 114–124.

Gu, H.Y., Hu, Z.X., Liu, D., Xiao, Y., Cheng, X., 2015b. Experimental studies on heat transfer to supercritical water in 2 × 2 rod bundle with two channels. Nucl. Eng. Des. 291, 212–223.

Gu, H.-Y., Hu, Z.-X., Liu, D., Li, H.-B., Zhao, M., Xu Cheng, X., 2016. Experimental study on heat transfer to supercritical water in 2 × 2 rod bundle with wire wraps. Exp. Therm. Fluid Sci. 70, 17–28.

Gupta, S., Saltanov, E., Mokr, S.J., Pioro, I., Trevani, L., McGillivray, D., 2013. Developing empirical heat-transfer correlations for supercritical CO2 flowing in vertical bare tubes. Nucl. Eng. Des. 261, 116–131.

Hofmeister, J., Schulenberg, T., Starflinger, J., 2005. Optimization of a fuel assembly for a HPLWR. In: ICAPP 05, Seoul Korea, May 15–19.

Hofmeister, J., Waata, C., Starflinger, J., Schulenberg, T., Laurien, E., 2007. Fuel assembly design study for a reactor with supercritical water. Nucl. Eng. Des. 237, 1513–1521.

Hu, Z-x., Gu, H-y., 2018. Heat transfer of supercritical water in annuli with spacers. Int. J. Heat Mass Transf. 120, 411–421.

Kong, X., Li, H., Zhang, Q., Guo, K., Luo, Q., Lei, X., 2019. A new criterion for the onset of heat transfer deterioration to supercritical water in vertically-upward smooth tubes. Appl. Therm. Eng.

Krasnoshchekov, E.A., Protopopov, V.S., Van, F., 1967. Experimental investigation of heat transfer for carbon dioxide in the supercritical region. In: Proceedings of the 2nd All-Soviet Union Conference on Heat and Mass Transfer. Minsk, Belarus.

Lei, X., Zhang, J., Gou, L., Zhang, Q., Li, H., 2019. Experimental study on convection heat transfer of supercritical CO2 in small upward channels. Energy.

Lemmon, E.W., Huber, M.L., McLinden, M.O., 2002. NIST reference fluid thermodynamic and transport properties—REFPROP. NIST Standard Reference Database 23, v7.

Li, H-b., Zhao, M., Hu, Z-x., Zhang, Y., Wang, F., 2018. Experimental study of supercritical water heat transfer deteriorations in different channels. Ann. Nucl. Energy 119, 240–256.

Liu, J., Jin, Y., Zhao, P., Ge, Z., Yuanjie Li, Y., Wan, Y., 2019. Analysis of heat transfer of supercritical water by direct numerical simulation of heated upward pipe flows. Int. J. Therm. Sci. 138, 206–218.

McAdams, W.H., Kennel, W.E., Addoms, J.N., 1950. Heat transfer to superheated steam at high pressures. Trans. ASME 72, 421–428.

Mokry, S., Pioro, I.L., Farah, A., et al., 2011. Developing of supercritical water heat-transfer correlation for vertical bare tubes. Nucl. Eng. Des. 241, 1126–1136.

Ornatsky, A.P., Glushchenko, L.P., Siomin, E.T., 1970. The research of temperature conditions of small diameter parallel tubes cooled by water under supercritical pressures. In: Proceedings of the 4th International Heat Transfer Conference. Paris-Versailles, France. Elsevier, Amsterdam.

Petukhov, B.S., Kurganov, V.A., Ankudinov, V.B., 1983. Heat transfer and flow resistance in the turbulent pipe flow of a fluid with near-critical state parameters. High Temp. 21, 81–89.

Pioro, I.L., 1 December 2019. Current status of research on heat transfer in forced convection of fluids at supercritical pressures. Nucl. Eng. Des. 354, 110207.

Pioro, I.L., Khartabil, H.F., Duffey, R.B., 2004. Heat transfer to supercritical fluids flowing in channels – empirical correlations (survey). Nucl. Eng. Des. 230, 69–91.

Podila, K., Rao, Y.K., 2014. CFD analysis of flow and heat transfer in Canadian supercritical water reactor bundle. Ann. Nucl. Energy 75, 1–10.

Policy Group, 2016. GIF Annual Report. OECD Nuclear Energy Agency.

Qu, M., Yang, D., Liang, Z., Wan, L., Liu, D., 2018. Experimental and numerical investigation on heat transfer of ultra-supercritical water in vertical upward tube under uniform and non-uniform heating. Int. J. Heat Mass Transf. 127, 769–783.

Schulenberg, T., Starflinger, J., 2012. High Performance Light Water Reactor, Design and Analyses. KIT Scientific Publishing.

Shen, Z., Yang, D., Wang, S., Wang, W., Li, Y., 2017. Experimental and numerical analysis of heat transfer to water at supercritical pressures. Int. J. Heat Mass Transf. 108, 1676–1688.

Shitsi, E., Debrah, S.K., Agbodemegbe, V.Y., Ampomah-Amoako, E., 2017. Numerical investigation of heat transfer in parallel channels with water at supercritical pressure. Heliyon 3 (11), e00453.

Shitsi, E., Debrah, S.K., Agbodemegbe, V.Y., Ampomah, 2018. Performance of heat transfer correlations adopted at supercritical pressures: a review. World J. Eng. Technol. 6, 241–267.

Shitsman, M.W., 1974. Heat transfer to supercritical helium, carbon dioxide, and water: analysis of thermodynamic and transport properties and experimental data. Cryogenics 77–83.

Waata, C.L., 2006. Coupled Neutronics/Thermal-Hyhdraulics Analysis of a High Performance Light Water Reactor Fuel Assembly.

Wang, H., Bi, Q., Wang, L., Lv, H., Leung, L.K.H., 2014. Experimental investigation of heat transfer from a 2 × 2 rod bundle to supercritical pressure water. Nucl. Eng. Des. 275, 205–218.

Wang, H., Bi, Q., Wang, L., Leung, L.K., 2017a. Non-uniform heat transfer of supercritical water in a tight rod bundle–Assessment of correlations. Ann. Nucl. Energy 110, 570–583.

Wang, H., Wang, W., Bi, Q., 2017b. Experimental investigation on boiling heat transfer of high pressure water in a SCWR sub-channel. Int. J. Heat Mass Transf. 105, 799–810.

Wang, Q., Song, Z., Zheng, Y., Yin, Y., Liu, L., Wang, H., Yao, J., 2019. Coupled convection heat transfer of water in a double pipe heat exchanger at supercritical pressures: an experimental research. Appl. Therm. Eng. 159, 113962.

Xi, X., Xiao, Z., Yan, X., Li, Y., Huang, Y., 2014a. An experimental investigation of flow instability between two heated parallel channels with supercritical water. Nucl. Eng. Des. 278, 171–181.

Xi, X., Xiao, Z., Yan, X., Xiong, T., Huang, Y., 2014b. Numerical simulation of the flow instability between two heated parallel channels with supercritical water. Ann. Nucl. Energy 64, 57–66.

Zahlan, H., Leung, L., Huang, Y., Liu, G., June 2018. General assessment of convection heat transfer correlations for multiple geometries and fluids at supercritical pressure. CNL Nuclear Rev. 7 (1).